Positive impedance and low hysteresis MOS type humidity sensors via SRCBD poly crystalline Sn_xO_y thin films

B. C. Anand [a,*], R. Shashidhar [b], N. Choudhary[c]
a Department of Physics, JSSATE Research Centre, JSS Academy of Technical Education, Bengaluru-560060 Karnataka, India
[b, c] Department *of Physics,*
JSS Academy of Technical Education, Bengaluru-560060 Karnataka, India

Resistivity-type humidity sensors have undergone extensive research as a result of the increasing demands in industry, agriculture, and daily life. Only a few carbon composites have been reported to exhibit positive humidity impedance, and the vast majority of humidity sensors currently in use are based on negative humidity impedance, in which electrical resistance increases as humidity levels increases. However, in this case, we only have fabricated positive impedance MOS type humidity sensors using SRCBD polycrystalline Sn_xO_y thin films. By changing the composition of x and y due to air annealing, the resistance of Sn_xO_y film sensors changes in response to relative humidity from a negative to a positive value. It was found that oxygen vacancy defects were the root cause of the positive humidity impedance. Positive humidity impedance sensors are more energy-efficient, simpler to miniaturize, and electrically safer than their negative counterparts as they operate at lower voltages, expanding the range of applications for humidity sensors. We also believe that by making vacancies in semiconducting materials, positive impedance humidity sensors can be made universally. A MOS device with low hysteresis was developed using Sn_xO_y films that were air annealed at 450°C and can be used as a reliable humidity sensor in a variety of applications.

1. Introduction

Resistivity-type sensor work on the principle of change in their electrical resistance as a function of atmospheric humidity. These novel characteristics of these sensors have attracted the wide attention of investigators due to its applications in agriculture, industry, and other day-to-day applications [1-5]. Most of the reported humidity sensors report work on the principle of negative humidity response in which electrical resistance is inversely proportional to humidity. However, humidity sensors have lower operational voltage, therefore, positive humidity impedance sensors are easier to be fabricated and electrically more stable, energy-efficient air humidifiers and more suitable for protectors for integrated circuits from humidity. But, for fabricating positive impedance humidity sensors, mostly carbon composites have been used and reported [6-8].

Semiconductor metal oxides have better response and better recovery time and higher sensitivity; therefore, it has been investigated widely for its use in the fabrication of potential solid-state chemical sensors [9-11]. Among them, Tin oxide semiconductors have been reported extensively due to its suitability in gas sensing, photocatalysis and electrochromism [12-14]. Additionally, Tin oxide semiconductors would be used as gas sensors for several gases such as H_2S, O_2, NO_x, CO_x, NH_3 and so on [15-18]. Numerous composite materials, such as poly-2,5-dimethoxyaniline/WO3 composites are used to functionalize humidity sensors. [21], some of them are the mixture of Cr_2O_3 and WO_3 [22], and polyaniline/WO_3 composites [23]. Among them WO_3 nanowire humidity sensor which has been fabricated using the CMOS-MEMS technique [19] and the thin film sensor fabricated using deposition techniques [20]. However, none of these have been

---

reported as positive impedance humidity sensors. The response of sensing mechanism against relative humidity in WO_3 may be attributed to the water dissociative chemisorption process in which hydroxyl groups are formed on the surface of the WO_3 crystal leading to the accumulation of electrons on its surface, and hence, the resistance of WO_3 crystal decreases with increase in relative humidity [21-24]. We have not found any literature reviews that mention the impact of metal oxide oxygen vacancies density on applications for relative humidity sensing.

Most oxygen-deficient oxides have been reported to be unstable in humid conditions, however, Sn_xO_y oxygen-deficient metal oxide have been reported with numerous advantages compared to its counterpart like the ease of synthesis due to their higher order of stability, ordered phases and precise stoichiometries [25]. Additionally, a literature review demonstrates that oxygen vacancy explains the level of defects and trap-assisted conduction in semiconducting oxides [26-29] and has been reported by Gillet and co-workers [29,30] that density of oxygen vacancy in Sn_xO_y may be influenced by water vapor if the experiment is performed in air. We have been motivated to create various Sn_xO_y humidity-assisted resistors because of these significant findings, in which the various oxygen vacancy densities may induce and modulate the humidity sensitivity.

In the present work, we have used Substrate Rotation Chemical Bath Deposition (SRCBD) technique to fabricate oxygen-deficient Tin oxide (Sn_xO_y) nanofilms in oxygen ambiance by coating Tin oxide thin films onto ITO substrates. The silver paste was used as an anode on the surface of the films and suitable electrical connections were made. The sensor prepared by polycrystalline Sn_xO_y films, notably showed positive humidity sensing property with a high density of oxygen vacancy. Additionally, by varying the atomic percentage of x and y in Sn_xO_y films the resistance may be tuned for the response of the relative humidity from a negative to positive. We believe that our method is novel for creating highly accurate positive humidity sensors using different metal oxides, and it opens a window to understanding and producing desirable semiconducting oxide humidity sensors. Additionally, research on the positive resistance characteristics of single-component material humidity sensors can balance and improve the principles of humidity sensing as well as expand the range of applications for humidity-sensitive resistors in small devices.

2. Experimental

2.1. SnO$_2$ thin film synthesis

In this study, SnO_2 thin films were deposited on pre-cleaned substrates using the SRCBD [Fig1] at 60°C and ambient pressure. The substrates such as glass and quartz were cleaned with soap, acetone, and chromic acid and finally with DI water. ITO substrate was cleaned with 10 % NaOH solution and DI water. However, the p-Silicon (100) substrate was cleaned using RCA-1, and RCA-2 solutions and finally, the native oxide on the silicon surface is removed by HF solution. All the cleaned substrates were dried in hot air and stored in Borosil desiccators to protect against any atmospheric exposure.
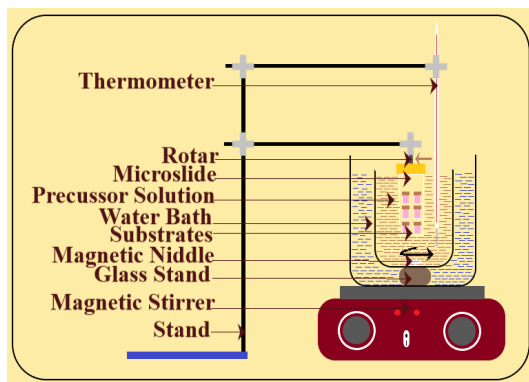

Fig. 1. Schematic of Substrate Rotation Chemical Bath Deposition (SRCBD).

A beaker containing 0.1 M Stannous Chloride dehydrates ($SnCl_2.2H_2O$) dissolved in 200 ml of DI water is placed in a preheated water bath and the solution temperature is maintained at 60^oC. To increase the solubility of the solution, 4.5ml of HCl is added to the solution under slow stirring with the magnetic niddle. Finally, 2ml of triethanolamine [$C_6H_{15}NO_3$] as a complexing agent and 5 ml of methanol (CH_3OH) was added to the solution to achieve homogeneity. The prepared solution was allowed to cool down to room temperature and its 10 pH was maintained by adding an appropriate quantity of ammonium hydroxide (NH_4OH) solution.

Again, the water bath is heated to maintain the solution temperature of 60^oC, and 0.1 M of Urea (CH_4N_2O) is added to the solution under continuing slow stirring. Pre-cleaned substrates were dipped vertically in the beaker containing the precursor solution and the rotation speed of the substrate holder was maintained at 30 rpm.

After the completion of 2 hours of deposition, the reaction vessels were left in the chemical bath for 24 hours to ensure better homogeneity. The films were removed from the solution and cleaned with DI water and dried under hot air using a hairdryer and again dipped into the same solution. This process is repeated several times to increase uniformity and film adhesion on the substrate.
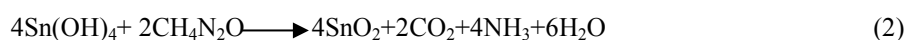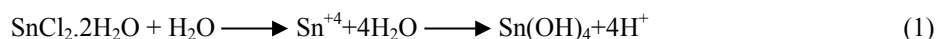
Finally, as-deposited (60^oC) SnO_2 thin films were air annealed in the muffle furnace at various temperatures of 300°, 350°, 400°, 450° and 500^oC for 60 minutes each, to further optimize crystallinity, stoichiometry, morphology, bandgap, sheet resistance, and other sensor parameters.

To investigate the influence of air annealing on microstructural, surface morphological, compositional, optical and electrical properties, and their utility as humidity sensors at room temperature, SnO_2 thin films have been subjected to various characterizations.

The structural properties of SnO_2 were characterized by X-ray diffraction (XRD, XPERT-3) RAMAN (LabRAM HR (UV) in the range of 100–1000 cm^{-1} and FTIR (PerkinElmer, Frontier) in the range of 4000 to 400cm^{-1}. Morphological and compositional properties were characterized by SEM with EDS (VEGA3 LMU) and film thickness by Microbalance (SHIMADZU BL series with a sensitivity of 0.1 mg) using the gravimetric method. UV-visible-IR spectroscopy (Shimadzu, MPC3600) in the range of 200–1100 nm, was used to measure the optical properties of the synthesized films and their thickness was estimated by the gravimetric method and compared with that by transmission studies. The sheet resistance of films was measured by the 2-probe electrical technique using MECO 603 multimeter and the impedance of the humidity sensor was estimated employing an LCR meter (APLAB 4910) at 100 Hz. To understand the reproducibility, the surface and electronic properties of each sample of present films were estimated at three or four positions.

2.2. Film Formation Mechanism

The formation mechanism of SnO_2 film has been presented in the below-mentioned equations. The $SnCl_2$ solution contains Sn^{4+} ions that hydrolyze to form $Sn(OH)_4$. On adding urea into the solution, SnO_2 thin film is formed on the substrates. On completion of one substrate rotation, the monolayer of a SnO_2 is formed. The desired film thickness of SnO_2 is controlled by rotating the substrate at 30rpm in the precursor solution for 2 hours and achieved by ageing the substrates in the solution for 24 hours. The obtained as-deposited films were subjected to air annealing to optimize the properties of the film as a function of thickness and its utility for gas sensing applications.

$$SnCl_2.2H_2O + H_2O \longrightarrow Sn^{+4}+4H_2O \longrightarrow Sn(OH)_4+4H^+ \tag{1}$$

$$4Sn(OH)_4+ 2CH_4N_2O \longrightarrow 4SnO_2+2CO_2+4NH_3+6H_2O \tag{2}$$

2.3. Thickness measurements (t)

The thickness (t) of the film is given by

$$t = \frac{(m_1 - m_0)}{A\rho} \tag{3}$$

where the substrate's masses (kg) before and after the film was deposited are denoted by m_0 and m_1, respectively. Stands for the film's surface area (m^2) and ρ for the bulk SnO_2's density (kg m^{-3}). Thus, the estimated film thickness (t) was found in the range of 154-502nm.

2.3. XRD analysis

The SnO_2 films have been annealed at various temperatures and their X-ray spectra have been plotted in Fig.2a which shows that the peak of Miller Indices belongs to SnO_2 and the presence of a sharp structural peak confirms the polycrystalline nature of the films. The synthesized films have a preferential orientation to the (1 1 0) plane and are polycrystalline with a tetragonal structure, according to the results of X-ray diffraction on the samples [JCP2 card No. 41-1445 (lattice parameters a = 4.738, c = 3.187)][31]. Due to the low surface energy of the SnO2 crystallites, which correspond to the densest packed plane, all films have (110) as their preferred orientation [32–37].
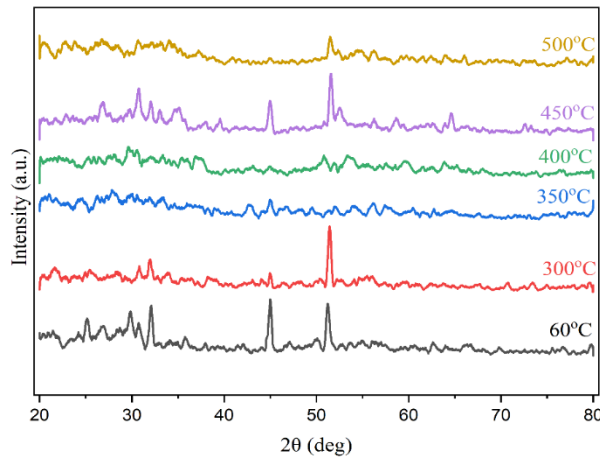

Fig. 2a. X-ray diffraction pattern of SnO₂ thin films.

Scherrer's formula [37] has been used to calculate the grain size of the crystallites given by

$$D = \frac{0.9\lambda}{\beta\cos\theta} \tag{4}$$

where D is the crystallite's grain size, the wavelength of the x-rays used is (λ=1.54059Å), the diffraction line's broadening is β measured in radians at half its maximum intensity, and the diffraction angle is θ.

The crystallite size estimated using Scherrer's equation at the preferred peak orientation was found to reach a minimum of 0.392 nm and the Stacking fault and d–spacing [Fig.2b] found by Bragg's law, tend to the maximum at 400℃ annealing temperature. The formation of SnO_2 films was confirmed by the diffraction pattern obtained from the calcinated complex at 400°C.

Table 1. Structural parameters of SRCBD: SnO$_2$ thin films estimated by both the Scherer formula and W-H method.

| Annealing temperature (^{o}C)	Modified Scherrer Equation			W-H Plot			Crystallinity %	Stacking faults
	Crystallites size D (nm)	Dislocation density δ (nm^{-2})	Micro Strain ε	Crystallites size D (nm)	Dislocation density δ (nm^{-2})	Micro Strain ε		
60 (as deposited)	2.2910	0.1905	0.0032	0.6213	2.5902	0.1419	23.4080	0.0498
300	5.0041	0.0399	0.0071	4.2324	0.0558	0.0919	25.2809	0.0605
350	0.9996	1.0007	0.0154	1.5759	0.4026	0.0455	27.6572	0.1180
400	3.6574	0.0747	0.0129	0.6991	2.0456	0.0501	31.3085	0.1050
450	2.6616	0.1411	0.0039	0.5778	2.9948	0.1430	36.6316	0.0470
500	3.2884	0.0924	0.0118	1.3307	0.5647	0.0051	38.2792	0.0899
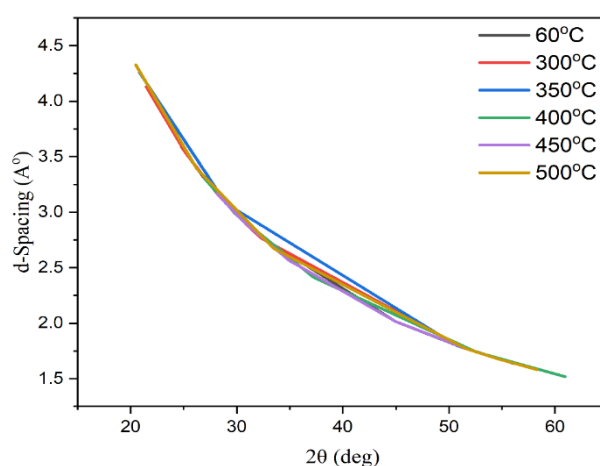
Fig. 2b. plot of d-spacing as a function of 2θ of SnO$_2$ thin films.

From table 1, it is observed that the percentage of crystallinity was found to increase with the annealing confirming the orderliness of the film. The crystallite size and dislocation density, Micro strain estimated from the W-H plot, was found to reach minimum and maximum at 450℃ annealing temperature.

The XRD peaks at 2θ= 30°, 33.5^o, 44.96^o and 51.42^o refer to (101), (110), (102) and (112) of SnO thin films [38]. The XRD peaks at 2θ= 25.19^o, 27.06^o, 30°, 33°, 51.8^o and 51.5^o refer to (001), (110), (111), (030), (300) and (310) of Sn$_2$O$_3$ thin films [JCPDS 25-1259] [39]. From the study at preferred orientation, it is observed that the at 60℃ synthesized films were SnO, however with an increase in annealing temperature films changes to SnO$_2$ at 400^{0}C and which again converts back to the mixed-phase of SnO and Sn$_2$O$_3$. The XRD peaks at 2θ= 31° and 44.96^o refer to Sn [40]. The XRD peaks at 2θ= 27.06^o, 34.93^o, 52.58^o, 54.55^o and 60.95^o refer to (110), (101), (211), (220) and (310) of SnO$_2$ thin films [JCPDS 41-1445] [41].

2.4. SEM Analysis

Air annealing was used to modify the microstructure [Fig.3] of the as-deposited SnO2 thin films, changing their mechanical and electrical properties. As a function of annealing temperature, it was observed that the average grain size ranged from 38.56 to 42.01 nm. The abnormal change in grain size may be attributed to the hydrolysis of urea and the disappearance of chlorine in the films. The grain size varies as a function of temperature due to completion of recovery and recrystallization in films, strengthening grain boundaries' resistance to intergranular cracks which

may, in turn, reduce hardness, increase ductility and help eliminate internal stresses. The annealing of films may also increase electrical conductivity monotonously due to minimization of dislocation density as a result of improvement of crystallization.
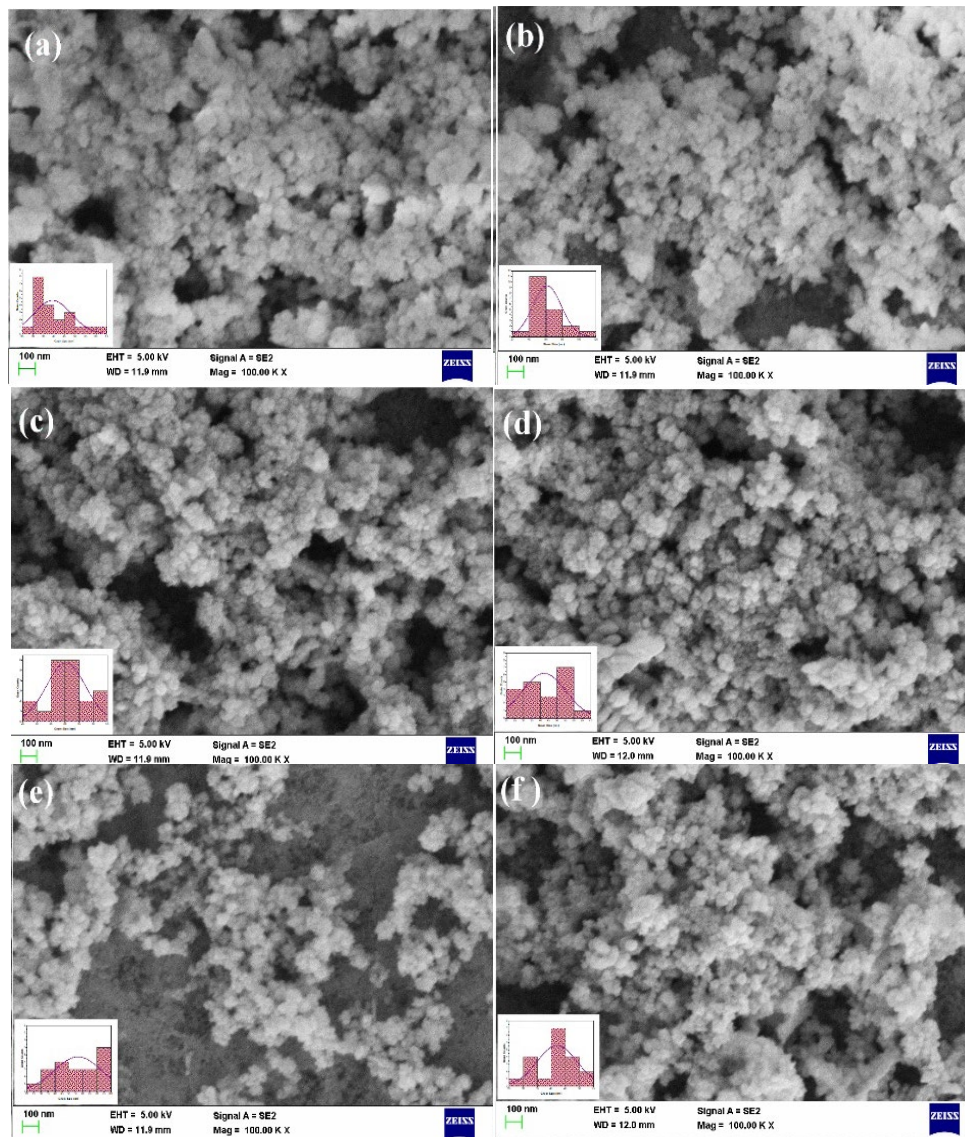

Fig. 3. SEM of as deposited and annealed SnO₂ thin films (a) 60ᵒC (b) 300°C (c) 350°C (d) 400° C
(e) 450°C (f) 500°C with grain size distribution histogram as inset.

2.5. EDS analysis (Chemical composition)

Energy Dispersive X-ray Analysis was used to characterize the SnO_2 thin films (EDS). Fig.4 displays the SnO2 thin film's EDS spectrum after being heated to 60, 300, 350, 400, 450, and 500°C. Additionally, it demonstrates the existence of a peak at 1.8 keV caused by silicon in the substrate used for film deposition. It also shows a well-defined peak for both tin and oxygen constituents of the above various substrate temperature SnO2 films, which confirms that the deposited films are indeed SnO2 and hence structural composition of the films are confirmed. In the samples, the oxygen element component (atomic %) is supposed to be twice that of tin, for confirmation of the chemical composition of SnO2 thin films.

Table 2 EDS analysis of elements and grain size estimated by SEM and histogram of SRCBD:SnO₂ thin films.

| Annealing temperature (°C)	Grain size (by SEM) (nm)	Grain size (by histogra) (nm)	Element - Weight %					Element - Atomic %					
			C K	Cl K	O K	Si K	Sn L	C K	Cl K	O K	Si K	Sn L	O:Sn
60 (as deposited)	55.70	38.56	7.98	1	33.45	2.48	55.08	19.9	0.85	62.7	2.65	13.9	4.51
300	51.84	61.50	9.35	1.10	29.76	2.71	57.08	24	0.95	57.3	2.98	14.8	3.87
350	41.88	40.32	13.12	0.72	24.7	24.38	37.07	28.48	0.53	40.23	22.62	8.14	4.94
400	37.54	42.29	8.28	----	29.11	23.07	39.54	18.82	----	49.67	22.42	9.09	5.46
450	64.03	56.49	3.73	----	32.79	22.08	41.4	8.88	----	58.7	22.5	9.98	5.88
500	46.77	42.01	5.83	----	30.57	28.28	35.32	13.11	----	51.64	27.21	8.04	6.42
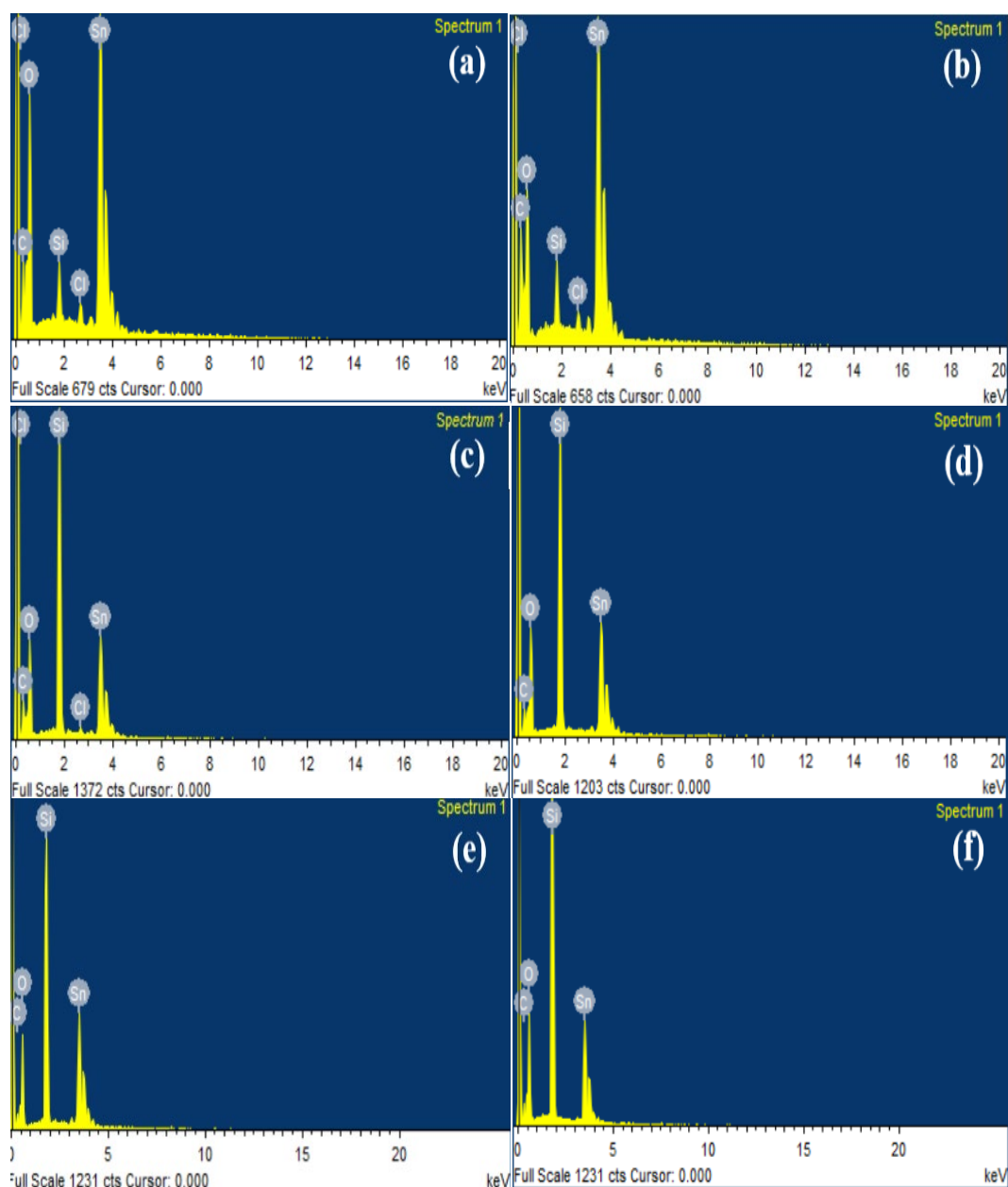
Fig. 4. EDS pattern of SnO2 thin films.

However, the Sn: O ratio [Table2] was found to vary from 0.16 to 0.26 % which is attributed to the hydrolysis of urea and the formation of SiO2 on the surface of the Silicon surface as a result of air annealing. Sn: O stoichiometry is very much less than 2, which may be due to the mixed-phase formation of SnO and Sn2O₃ along with desired SnO2 thin films. Both Sn and O atomic % were found to reach their minimum values at an annealing temperature of 350°C. At the exposed sites of the substrate, the silicon element is also observed in the EDS studies which may be due to the evaporation of unreacted precursors from the surface of the silicon substrate leaving vacant sites in that region. Due to the usage of urea as a precursor for the synthesis of film, Carbon element is detected in the studies; however, its content keeps decreasing as a result of hydrolysis of urea due to enhancement of annealing temperature. Chlorine is also found in the film due to the usage of HCl for complete solubility of precursor, whose content was found to disappear after an annealing temperature of 350℃. No other impurities are detected confirming the high purity of the SnO2 thin film.

2.6. Raman Studies

Since Raman spectroscopy is best suited for analyzing solids and because Raman bands are directly caused by molecular vibrations, which are sensitive to changes in composition, stoichiometry, and structure, samples that were deposited and air annealed were studied. To further verify phase formation and the deposition of SnO_2 thin films over a silicon substrate, 100 to 1000 cm-1 at room temperature Raman spectra were collected. The results are shown in Fig.5 It is a very helpful technique to describe the potential vibration modes in any material as a reflection of its purity and phase. Raman spectra with variation in the oxidation temperature as shown in the figure. After the oxidation process, the metallic tin (Sn) can be oxidized into tin monoxide (SnO) and/or tin dioxide (SnO_2) depending on the oxidation temperature.

Raman intensity was found to decrease at 300^{0}C, and reach a maximum at 350^{0}C with a further increase in annealing temperature was found to decrease and reach a minimum at 500^{0}C. The maximum intensity of the peak is due to the increment of crystal size. A minimum at 500^{0}C is attributed to non-stoichiometric tin dioxide SnO_{2-b} [43], and the decreased peak intensity with annealing is attributed to the change in phase [42]. The Raman modes in the low-wavelength region decreased and disappeared as the oxidation temperature rose to 500^{0}C, indicating a reaction toward stoichiometric SnO_2 [44].

No prominent peaks were seen for oxygen-deficient as-deposited films. However, with air annealing major peaks were observed at 516 cm^{-1} for 350^{0}C, 300^{0}C annealed films, and at 520 cm^{-1} for 450^{0}C, and 400^{0}C annealed films. Among the peaks, Intensity is found to be minimum at 400^{0}C and maximum at 450^{0}C annealed temperature respectively. Minor and major peaks were observed for 400^{0}C and 450^{0}C annealed films. A minor peak is caused by an oxygen vacancy (VO) or oxygen defect in the deposited SnO2 thin films [45]. Beyond 350^{0}C, it is observed that the Raman peak changes from 516 cm^{-1} to the higher wavenumber 520 cm^{-1}.
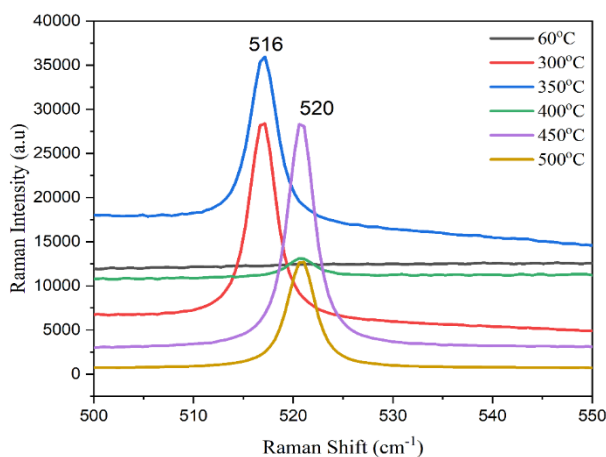

Fig. 5. Raman Spectra of SnO₂ thin films.

Thangadurai et al. reported that stressed SnO_2 (under pressure) exhibits Raman peaks at higher values in comparison to ambient conditions [46].The appearance of Raman peaks at relatively higher wavenumbers in the case of as-deposited films can therefore be inferred to be primarily caused by residual stresses, rather than non-stoichiometry[47].

The strain-induced shift of the first order 520 cm^{-1} Raman peak associated with optical phonons in silicon has been used to spatially map stress variations using Raman spectroscopy with a lateral resolution of a few nm. [48,49].

The length of molecules' chemical bonds in Raman spectra is related to the shifting of peaks toward higher wavenumber. The shorter bond length causes a wavenumber shift to a higher one or vice versa due to the variation in particle size and the change in molecule bond length. The formation of nanocrystals inside SnO_2 thin films is responsible for the sharp peak.

The band at 520 cm^{-1} is a Raman forbidden B_{1u} mode, whereas the Raman bands at 516 cm^{-1} can be assigned as A_{2u} (TO) mode, which is IR active. The characteristics of SnO_2 nanostructures are represented by these abnormal Raman bands, which were not visible in the Raman spectrum of bulk SnO_2. [50].

The Raman scattering peak at about 520 cm^{-1} was identified as that of the silicon substrate.

2.7. FTIR Studies

FT-IR spectroscopy is used to identify the adsorbed functional group from their frequencies. Fig.6 shows the FTIR spectra for SnO_2 film recorded between 400 and 4000cm^{-1} at room temperature. FTIR spectra of SnO_2 reveal that films have major bands at 3431, 2920, 2848, 1618,608 and 506 cm^{-1}[51]. The broadband has been observed at 3365 to 3620cm^{-1}and 1618 cm^{-1}which may be attributed to the absorption of water molecules from the environment during the synthesis of the films and consequently formation of stretching vibration mode of Sn-OH group and O-H stretching vibrations [51]. The presence of a band between 2848 and 2920 cm^{-1}may be attributed to the formation of the C-H group. There may be Sn-O stretching vibration and O-Sn-O bending vibration in the peak area, which is between 500 and 650 cm^{-1}. The formation of SnO_2 nanoparticles is confirmed by the presence of the aforementioned bands [51,52].
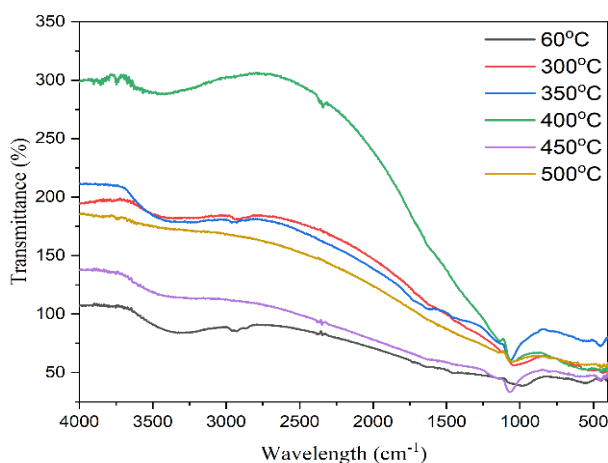

Fig. 6. Fourier Transform Infrared (FTIR) spectra of SnO$_2$ thin films.

Metal oxide bond of SnO_2 may be attributed due to the presence of bands between 400-800 cm^{-1}and 800-1700 cm^{-1} bands may be attributed to oxygen stretching and bending frequency. A SnO_2 nano thin film's infrared spectrum for annealing at 500^{0}C revealed specific peaks at 3425, 1625, and 615 cm^{-1}. The spectrum shows that the spectrum is clearest at the highest annealing temperature. The presence of a band around 3400 cm^{-1} may be explained by the $^-$OH functional group, which is present and becomes wider at lower annealing temperatures [53].

With the increase in annealing temperature, the transmission in the film was found to increase till 400^0C, however, at 450^0C the transmission was found to decrease later with a further increase in temperature up to 500^0C the transmission was again found to increase. The variation of transmission may be due to the desorption of adsorbed moisture from the surface of the film.

FTIR study indicated the existence of two distinct characteristic absorptions which correspond to (O- Sn-O) deformations and (O-Sn) stretching modes [54].

Two large peaks around 3444 and $1624 cm^{-1}$ are observed due to the vibrations of the hydrogen bond involved in the O-H oscillators in the adsorbed water molecules and the alcohol respectively [55] and small peaks around 1023, 1384 and $2356 cm^{-1}$ denote the hydrogen bonds involved in O-H oscillators and peaks around 2894 and $2353 cm^{-1}$ may be due to the CO_2 absorption from the ambient air atmosphere [56-58]. And two bands appearing around 574 and $665 cm^{-1}$ are due to the Sn-O-Sn vibration and the Sn-O bond in SnO_2 which confirms the existence of SnO_2 [59-61].

2.8. UV-VIS studies

Substrate rotation chemical bath deposited thin films were annealed at different temperatures (300, 350, 400,450, 500) °C in air for 60 minutes. Optical properties were also studied for annealed and unannealed (60^0C) films using UV-visible spectroscopy (model). Fig.7&8 shows the transmission and absorption spectrum of SnO_2 deposited on a quartz substrate. The spectrum is obtained as a function of the wavelength (200-1100 nm). From the graph It is observed that the transmission increases sharply at the beginning of the visible region and reaches the average maximum value of (90%) however at the end of this region near the IR, the curve oscillates due to interference effects in the thin film. In this study, the envelop method was used to calculate the film's thickness and refractive index. The thicknesses of the films were estimated by optical interference technique using wavelengths at maxima and minima and applying the envelop method equations. From the plots, it is evident that the surface quality and homogeneity of the thin film were excellent [62].

The experimental data are represented by the solid curve with the associated symbol. Strong absorption and high transmission are the two regions that make up the spectra's overall pattern. Between 400 and 1100 nm, there is a region of high transparency with transmission values of 78 to 93%. This value applies to our thin layers made by SRCBD and shows that the SnO2 thin films are transitive in the visible region. The transmission spectra showed higher transparency over the visible wavelength region with a maximum value (78-93) % depending upon annealing temperature. Low defect density and reduced optical film scattering are the causes of the high transmission [63].
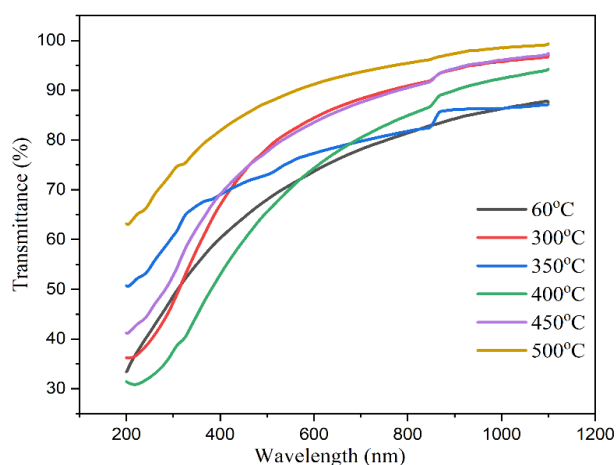

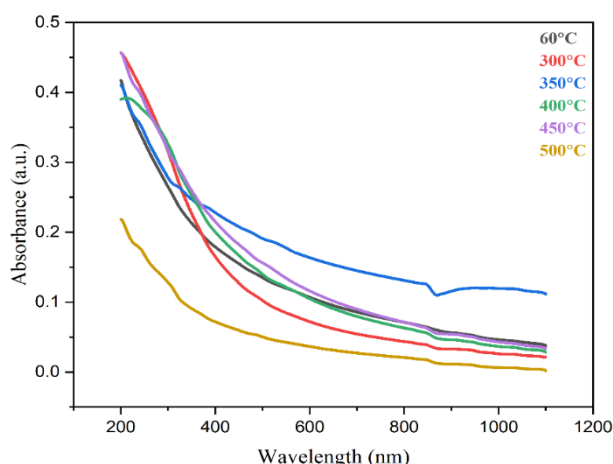*Fig. 7. Optical Transmittance spectra of SnO₂ thin films.*

Fig. 8. Optical Absorbance spectra of SnO₂ thin films.

The optical parameters extracted by the experimental transmission and absorption data are listed in Tables 3 & 4. From the transmittance plot, it is observed that the transmission in the film was found to increase with the air annealing due to a decrement in film thickness which may be attributed to an increment in grain size in the preferred orientation plane. The increment in the transmission is attributed to the decrease in free charges in SnO2 films may be due to oxidation and removal of oxygen vacancies as a result of air annealing of films. The prepared and annealed film's calculated absorption coefficient, which may be appropriate for a transparent conducting film, is in the range of 104 cm-1. However, the ultra-thin tin oxide film might not work as a transparent conducting film because the resistance of annealed film increases with a decrease in film thickness [64].

Table 3. Optical constants estimated by Transmission spectra of SRCBD: SnO₂ thin films.

Annealing temperature (^{o}C)	T nm	n	α /m	k	Φ %	T %	σ	χ	ε_r	P %
60 (as deposited)	410	1.4359	601948.3390	0.0335	64.6019	78.1297	2.0635E+13	0.0844	2.0608	0.5228
300	361	1.5226	343330.5128	0.0191	56.0545	88.3430	1.2480E+13	0.1048	2.3179	0.6105
350	266	1.5244	849652.7684	0.0473	55.8700	79.7712	3.0921E+13	0.1051	2.3216	0.6123
400	181	1.5313	1196835.5867	0.0666	55.1674	80.5230	4.3753E+13	0.1066	2.3405	0.6190
450	104	1.5263	1289486.6222	0.0718	55.6726	87.5625	4.6988E+13	0.1054	2.3246	0.6142
500	84	1.5230	775352.8549	0.0431	56.0074	93.6945	2.8192E+13	0.1048	2.3179	0.6110

Table 4. Optical constants estimated by Absorbance spectra of SRCBD:SnO₂ thin films.

Annealing temperature (^{o}C)	t nm	α /m	K	Σ	χ	ε_r	$(\alpha h\nu)^2$ $(eV\,m^{-1})^2$	$(\alpha h\nu)^{1/2}$ $(eVm^{-1})^{1/2}$
60 (as deposited)	410	282522.17	0.0157	9.6850E+12	0.0844	2.0616	4.05825	2.955
300	361	178709.51	0.0099	6.4960E+12	0.1049	2.3182	3.81224	2.59256
350	266	477497.44	0.0265	1.7377E+13	0.1052	2.3231	3.96192	2.51105
400	181	261920.19	0.0145	9.5752E+12	0.1070	2.3447	3.52621	2.36878
450	104	295468.32	0.0164	1.0766E+13	0.1058	2.3295	3.95747	2.37175
500	84	88849.74	0.0049	3.2306E+12	0.1050	2.3197	3.99452	2.40287

Refractive index, porosity, optical susceptibility, dielectric constant and magnitude of polarization were found to increase with annealing reaching a maximum at 400^0C, and decrease with further increase in temperature. Due to the high porosity of the SnO_2 film, its refractive index rises monotonically as thickness decreases. As a result, it is possible to assume that thinner films have smaller grains. The increase in inhomogeneity and surface roughness of the films could be to cause a higher value of the refractive index [65].

The absorption coefficient, extinction coefficient and optical conductivity were found to decrease at 300^0C and increase with further annealing, reach a maximum at 450^0C, and decrease with further annealing.

The optical direct bandgap (Fig.9) of the film was found to reach a minimum at 300^0C and 400^0C, however, the indirect bandgap (Fig.9) of the film reaches a minimum at 400^0C. From the optical study, it is observed that both the direct (4.05 to 3.52 eV) and indirect bandgap (2.95 to 2.36 eV) of the film is found to be affected by air annealing. The smaller bandgap and donor-acceptor recombination may be caused by the electronic transition from the deep donor level, which is created by the oxygen vacancies, to the valence band in the film. [66]. The value of the bandgap obtained is by the known value of SnO_2 [67,68]. Absorbed oxygen from air during annealing fills the oxygen vacancies and oxidizes the interested tin atom in the crystal structure which may lead to a variation of the optical bandgap of thin films [69,70].
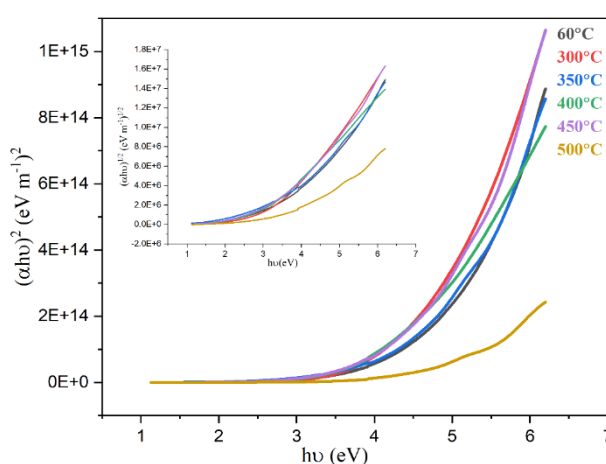

Fig. 9. Plot of $(\alpha h\nu)^2$ as a function of $h\nu$ [$(\alpha h\nu)^{1/2}$ as a function of $h\nu$ (inset).

3. Fabrication of MOS device

SnO_2 thin films were deposited by the SRCBD technique onto various precleaned substrates like glass, quartz, silicon, and ITO at 60^0C. As-deposited films were further air annealed from 300^0C to 500^0C for 60 minutes to understand the annealing effects on humidity sensing properties of MOS sensor. Films deposited on ITO were used to fabricate MOS devices, which were then tested as humidity sensors and had their electric properties tested. Shamala et al. have researched and reported on the fabrication of MOS capacitors and their dielectric properties. [71]. The following process was used to create Metal Oxide Semiconductor (MOS): On cleaned ITO substrates measuring 1 cm x 1.5 cm, SnO_2 thin films were applied. A 1 mm-diameter dot of silver epoxy was created and placed on the surface of the SnO_2 film. One more silver epoxy dot was created on the unmasked side of the ITO, and two leads were extracted for measurement purposes from these dots using thin copper wires. Fig.10a and Fig.10b provide the device's schematic and energy level diagram respectively. The gravimetric method was used to measure the film's thickness, and it was confirmed by transmission spectra of films deposited on ITO substrates. The MOS device's response to humidity is investigated using a homemade dehumidifier [Fig.11].

Using an LCR meter (APLAB 4910) operating at 100 Hz, the impedance of SnO_2 films deposited on ITO substrates was investigated.
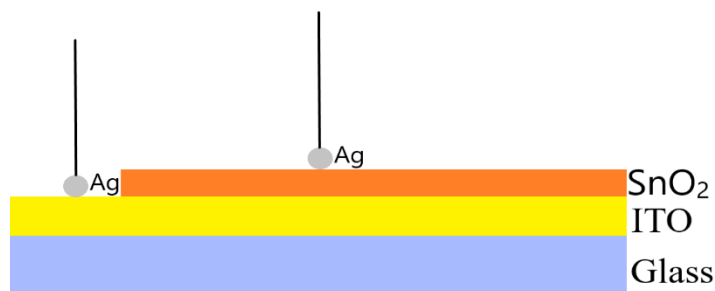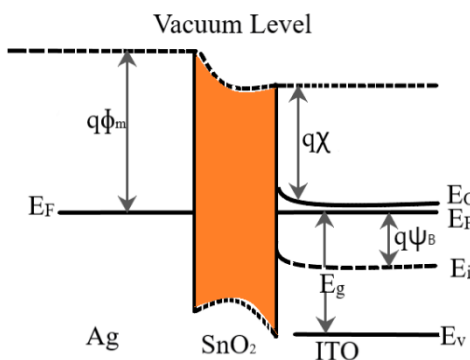

Fig. 10. (a) Schematic diagram of the SnO₂ MOS device.

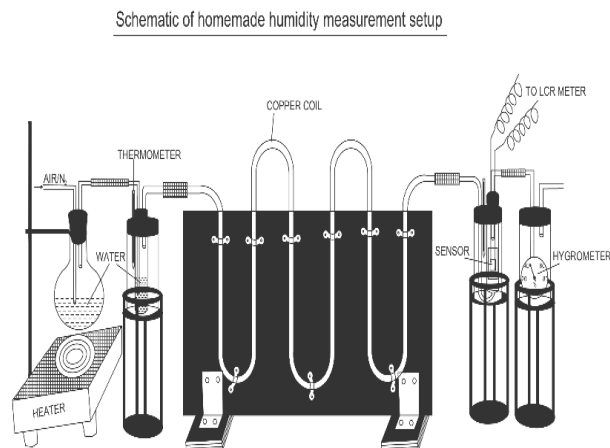*Fig. 10 (b) Energy band diagram of MOS before voltage application.*

Fig. 11. Schematic of the homemade humidity measurement setup.

3.1. Impedance versus RH percentage for MOS sensor

Because these films have a higher band gap (3.57 eV) and dielectric constant (9.86), they were used to fabricate the MOS sensor and were air annealed at various temperatures. SnO_2 films have a thickness of about 154-502 nm. With the aid of existing literature, a home-made sensor setup was created with the study of the variation of resistance with the percentage change in relative humidity (RH) for SnO_2 MOS sensor [72] and is shown in Fig.12. Air compressor, copper

helical tubes, two airtight glass jars, sensor holder, LCR meter, and hygrometer are the components of the relative humidity measurement setup.

By blowing hot air through the tubes, we were able to reduce the relative humidity to almost zero. However, when we bubbled water with compressed air, the relative humidity rose to 95%, and a corresponding increase in impedance was observed. The impedance was found to increase gradually at low RH values (0–20%) and moderately at medium RH (25–50%) before increasing quickly up to 90% RH, as shown in Fig.12. For all measurements, the humidity chamber's sensor's temperature was held constant at (27°C).

Nahar et al.,[73] however, measured the sensor characteristics at low humidity by enclosing the sensor in glass tubes filled with sulfuric acid solutions of known humidity. The variation of impedance with low and medium (0-50%) RH values as observed by us is precisely like that found by Jingwen Qian et al., except for the saturation part at high relative humidity found in our case [74].

It was observed that the impedance increases gradually at low RH values (0-20%), moderately at medium RH (25–50%), and then quickly up to 90% RH. Due to the higher density of oxygen vacancies in tin oxide films, which is comparable to the conduction behavior of many semiconducting oxides, the impedance of the sensors is low in low-medium humidity environments [75]. This phenomenon can be explained by the fact that oxygen vacancies are the locations of positive charges that easily attract electrons and bind them to them. As a result, the conductivity of semiconducting materials can be improved with an increase in oxygen vacancy density. The sensors' impedance exhibits a 100% positive resistance sensitivity to relative humidity (50–95%). The variation in grain size, improvement in film crystallinity, and stoichiometry of annealed films were found to result in lower impedance with decreasing oxygen vacancy density in tin oxide films.

In conclusion, the density of oxygen vacancies in the sensing materials has an impact on the humidity sensitivity of the sensors made with the currently structured tin oxide films, as shown by EDS elemental stoichiometric analysis. The sensors may exhibit full or partial positive humidity sensitivity across the entire RH range due to high or low oxygen vacancy densities in SnO2 thin films.
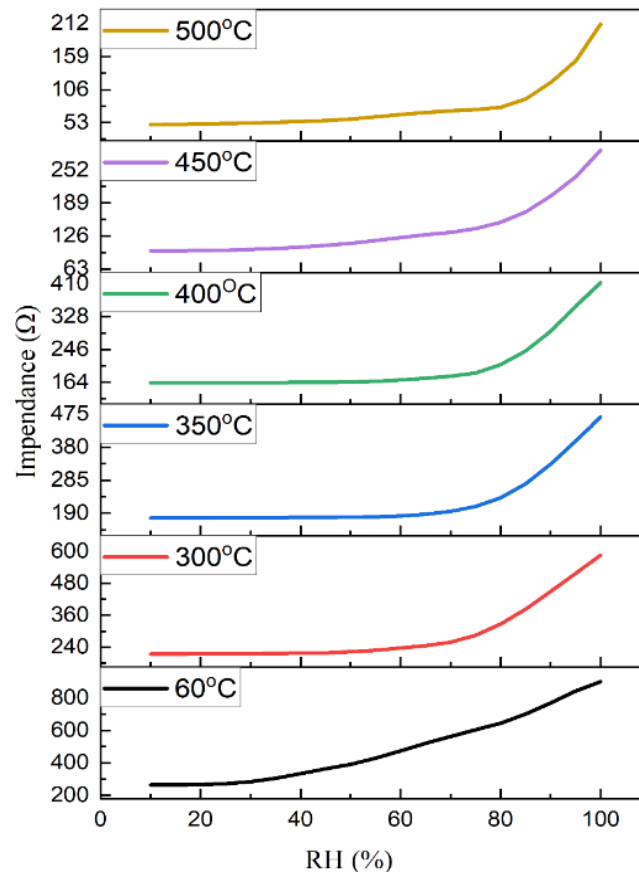
Fig. 12. Sensor Impedance as a function of Relative Humidity (%).

3.1.1. Responsivity (R)

The Responsivity (R) is recorded by exposing the fabricated MOS sensor to humidity. The sensitivity towards humidity can be confirmed by calculating the relative sensor response given by

$$Response\ (\%) = \frac{R_g - R_a}{R_a} \times 100 \tag{5}$$

where R_g and R_a are the resistance/impedance of the sensor in humidity and air, respectively. The Responsivity of SnO_2 based MOS sensor during adsorption and desorption of humidity as a function of annealing temperature is shown in fig.13a,13b

During adsorption-desorption processes in the range of 10-30 % RH, it is observed that the sensitivity was found to decrease and reach minimum for films annealed at 400°C, further the sensitivity was found to increase and reach maximum for films annealed at 500°C. Responsivity measured during desorption was found to be higher than that for adsorption. Films annealed at 500°C were observed to possess responsivity higher than that for as-deposited films confirming the effect of film annealing on the sensitivity of sensors. The Responsivity of the SnO_2-based MOS sensor during desorption is higher than that while adsorption of humidity due to deficiency of oxygen vacancies in the active region.

Sensitivity (S): It is possible to express the humidity sensors' sensitivity S as

$$S = \frac{I_{90} - I_{10}}{90 - 10}\ (\Omega/\%RH) \tag{6}$$

where I_{90} and I_{10} stand for the impedance measured at 90% and 10% relative humidity, respectively, the highest and lowest RH values in the variation range are 90 and 10. The fact that the sensitivity is found to be declining with air annealing may be due to grain size variation.
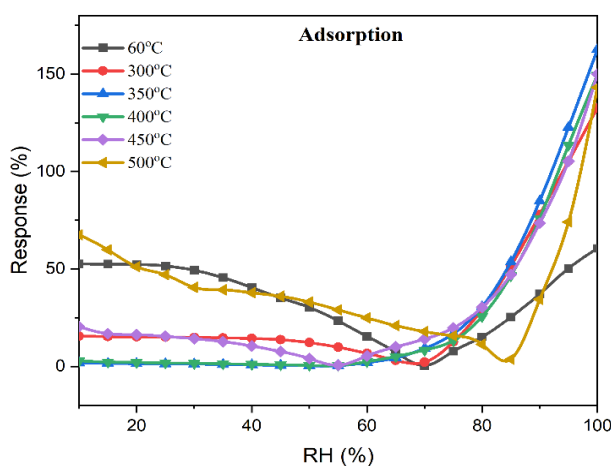
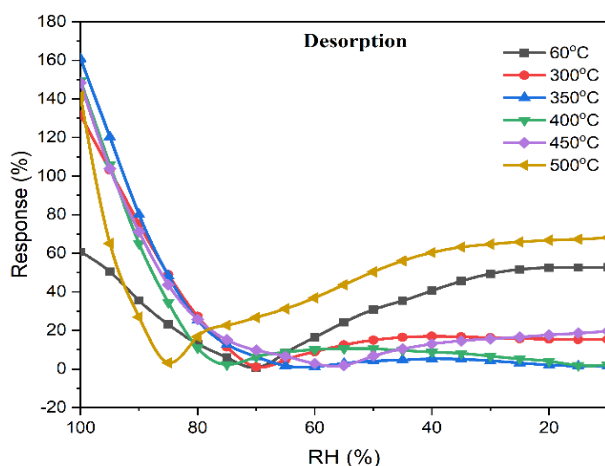*Fig. 13a. Responsivity of SnO₂-based MOS sensor during adsorption of humidity as a function of annealing temperature.*

Fig. 13b. Responsivity of SnO₂-based MOS sensor during desorption of humidity as a function of annealing temperature.

3.1.2. Hysteresis studies

For humidity sensor hysteresis is one of the essential characteristics, therefore, we have performed both adsorption and desorption hysteresis characteristics of synthesized films and as shown in Fig.14. The adsorption process RH was measured from low to high and has been shown in the red line black line indicates for desorption process which has been measured in the opposite direction. The increasing RH (for the adsorption process) and decreasing RH (desorption process) curve has been represented by the upper and lower curve respectively and these curves are very close to each other as shown in the figure. The impedance of a SnO_2-made sensor was observed to increase with increasing humidity, and the pathway for its desorption process was found to be higher up in the loop, indicating that the rate of desiccation of the adsorbed water was slower than that of adsorption, which is in good agreement with the response and recovery characteristics of a humidity sensor.

Films annealed at 400°C have the largest hysteresis loop area, and films annealed at 450°C have the smallest. The maximum hysteresis loss may be caused by small grain size, porosity, or domains, while the minimum hysteresis is attributed to larger grain size and porosity in films. In films rich in small grains, desorption is slower than adsorption, and vice versa in films rich in larger grains.

$$H = \frac{I_D - I_A}{S} \,(\%RH) \tag{7}$$

where I_D and I_A are, respectively, the desorption and absorption processes' Impedance values as measured at 50% relative humidity. According to calculations, the humidity sensor has a maximum hysteresis H of 1536.15% RH (400°C) and minimum hysteresis is 192.33% RH (60°C) at 50% RH. [Table 5]. This outcome provides strong evidence that air annealing lowers the hysteresis value.

One of the main issues with resistive humidity sensors is hysteresis. The presence of water clusters may deform the ITO, which will affect the sensor's performance. Due to its larger grain size, SnO$_2$ films air annealed at 450^{0}C were found to exhibit lower hysteresis. Ionic conduction theory can be used to explain the role of the SnO$_2$ nanoparticles. [76] The SnO$_2$ nanoparticles can adsorb water molecules to form hydroxyl groups on their surfaces. When additional water is added, each water molecule forms a liquid-like layer of hydrogen-bonded water molecules where each water molecule is only singly bonded to a hydroxyl group. This technique effectively suppressed the water clusters on the ITO, resulting in low hysteresis.
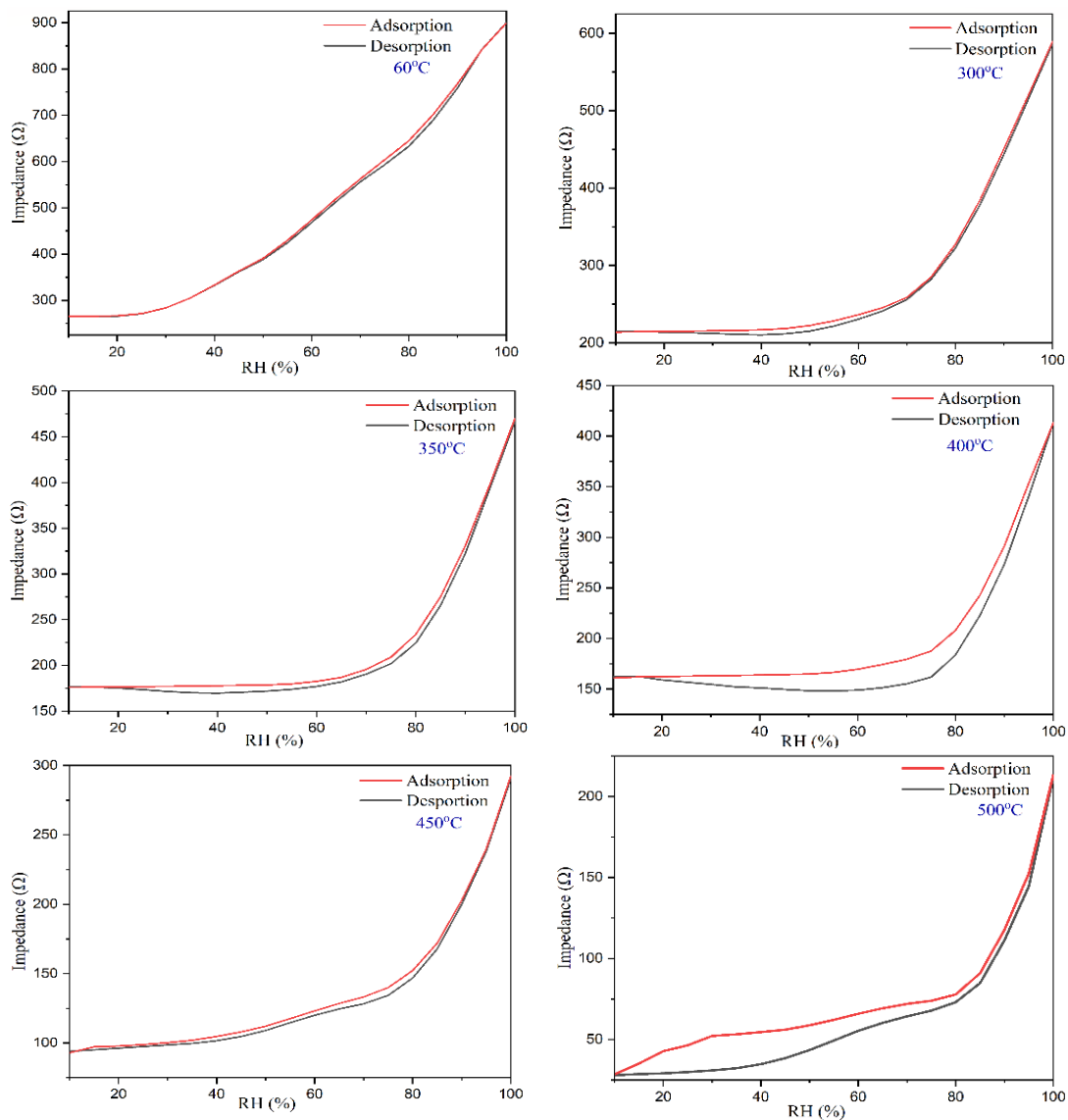

Fig. 14. The hysteresis curve during both adsorption-desorption processes of tin oxide-based humidity sensors.

Table 5. Sensitivity parameters of SRCBD: SnO₂ thin film Humidity sensor.

Annealing temperature (^{o}C)	Sensitivity (S) (Ω/%RH)	Drift (%RH)	Hysteresis by graph (%RH)	Hysteresis by formula (%RH)
60 (as deposited)	6.28	27.00	371.90	192.33
300	2.96	10.47	392.68	236.43
350	1.94	0.28	511.06	488.37
400	1.63	0.56	1301.78	1536.15
450	1.37	3.44	267.47	400.91
500	1.12	25.92	1020.07	1900.42

3.2. Response and recovery time for MOS sensor:

We have examined the SnO₂ film's response and recovery characteristics over a single cycle, which corresponds to the processes by which water molecules adsorb and desorb. This cycle is demonstrated by a sensor reaching 90% of the total impedance change as humidity increases from 11 to 95% RH and reaching 90% of the total impedance change as humidity decreases in the opposite direction and range, respectively. Their statistical response and recovery times are shown in Fig.15. It may be observed that the sensor is extremely sensitive to the variation of environmental humidity as both response and recovery time changes drastically which may be attributed to the variation of densities of oxygen vacancies in the sensing SnO₂ films [77]
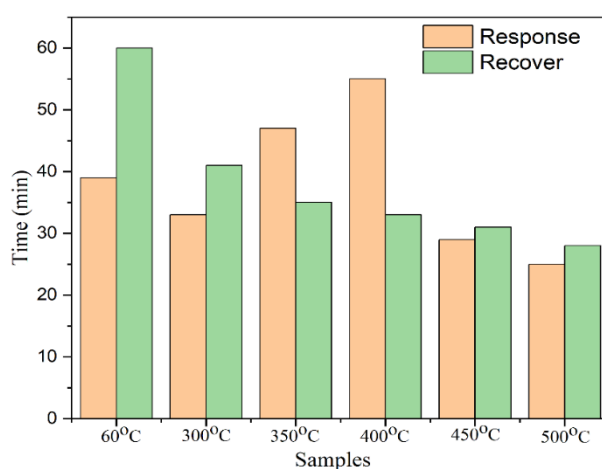

Fig. 15. Statistical response and recovery times of the humidity sensors fabricated with the obtained SnO₂ thin films.

From the plot it is observed that the recovery time was found to decrease with annealing, however response time was found to reach maximum for films annealed at 400^{0}C, with further increase in temperature, time is on decreasing trend. As evident from the hysteresis curve, lower recovery time in annealed films might be due to the fast desorption of water molecules from the film surface. The longer adsorption of water molecules at the film surface may be the cause of the maximum response time in films that were annealed at 400^{0}C. Improper water-porous humidity interaction MOS humidity sensors may exhibit hysteresis because of sensitive layers. An increased contact area between the sensing layer and the water vapor due to the porous top electrode may result in high sensitivity and rapid response [78].

3.3. Stability

For an ideal humidity sensor, stability is one of the important properties in practical applications. To understand the stability of the MOS sensor, impedance is again estimated for 100 days in a step of 20 days. All samples were exposed to air for a few minutes, and the corresponding impedance is recorded. The impedance variation of the sensor with time, when exposed to air is shown in Fig.16. It is observed that all the films exhibit excellent reproducibility even after exposure to air after 100 days also, with slight deviations. The initial Impedance (in ohm) values were around 560.1. 253.3, 179.1, 165.6, 116.8 and 87.6 which are decreased to 580.3, 265, 179.8, 168.1, and 119, 89.5respectively after 100 days of film exposure. The slight variation in the impedance after long storage (exposure) times is due to the oxygen attack on the conjugated double-bond system [79].
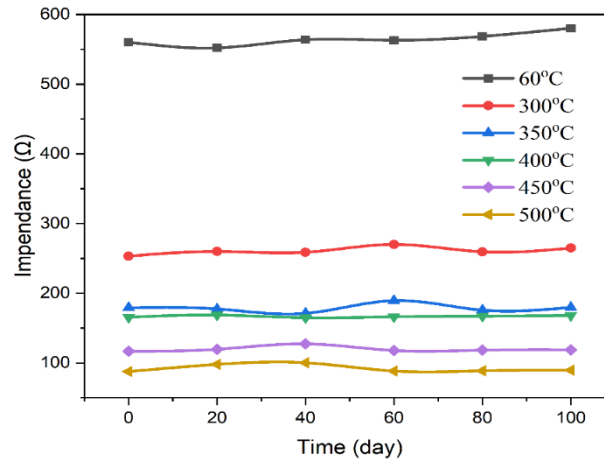

Fig. 16. Stability studies of the MOS sensors fabricated with as-deposited and annealed SnO_2 thin films.

The apparent changes in relative humidity, D, which are calculated by the sensor resistance drift's magnitude is estimated by [80]

$$D = \frac{I_{(meas)} - I_{(init)}}{S} \quad (\%RH) \tag{8}$$

where $I_{(meas)}$ is the measured impedance following the sensor's exposure to a 50% relative humidity environment for a predetermined amount of time, and $I_{(init)}$ is the initial impedance before the test.

At 50% relative humidity, the highest [60°C] drift value was 27% RH. However, the drift value has decreased to a minimum [350°C] of 0.28% RH [Table 5] with air annealing as a result, the sensor is an extremely promising candidate for a commercially available humidity sensor from a practical standpoint. As a result, from a practical standpoint, the sensor has attained notable stability and is a very promising candidate for a commercially available humidity sensor.

4. Conclusion

On a variety of substrates, including glass, quartz, silicon, and ITO, SnO_2 thin films were created using the SRCBD method in order to study their electrical characteristics in relation to humidity sensors. SnO_2 thin films' structural, morphological, optical, and electrical characteristics were examined in both their unannealed and air-annealed states. As humidity sensors, MOS devices were fabricated and tested. Impedance variation is investigated with RH. When the humidity level is low, the MOS sensor exhibits a slow increase in impedance, a medium increase at medium RH, and a rapid variation at high RH levels. In conclusion, using SRCBD

polycrystalline Sn_xO_y thin films, we were able to create positive impedance humidity sensors that were driven solely by oxygen vacancy defects. Positive humidity impedance sensors would, from an industrial perspective, be safer electrically, more energy-efficient, and simpler to miniaturize than their negative counterparts. The fabricated sensor showed improved response sensitivity, decreased hysteresis, a quicker response/recovery time, excellent repeatability, and good long-term stability. Finally, it was demonstrated that a good resistance value that is temperature dependent, stable, and has a slight drift is adequate for use in a dependable humidity sensor for a variety of applications.

Acknowledgments

References

[1] Hong-Tao, Sun, Wu Ming-Tang, Li Ping,Yao Xi, Sensors and Actuators. 19(1) (1989)61-70; https://doi.org/10.1016/0250-6874(89)87058-1
[2] Chen, Zhi, Chi Lu, Sensor letters 3(4) (2005) 274-295; https://doi.org/10.1166/sl.2005.045
[3] Qi, Qi, Tong Zhang, Qingjiang Yu, Rui Wang, Yi Zeng, Li Liu, Haibin Yang, Sensors and Actuators B: Chemical 133(2) (2008) 638-643; https://doi.org/10.1016/j.snb.2008.03.035
[4] Wang, Rui, Xiangwei Liu, Yuan He, Qing Yuan, Xiaotian Li, Geyu Lu,Tong Zhang, Sensors and Actuators B: Chemical 145(1) (2010) 386-393; https://doi.org/10.1016/j.snb.2009.12.025
[5] Sundaram, R., K. S. Nagaraja, Materials research bulletin.39(4-5) (2004) 581-590; https://doi.org/10.1016/j.materresbull.2003.12.014
[6] Li, Yang, Lijie Hong, Yousi Chen, Huicai Wang, Xin Lu, Mujie Yang, Sensors and Actuators B: Chemical 123(1) (2007) 554-559; https://doi.org/10.1016/j.snb.2006.09.057
[7] Jiang, Wei Fen, Shun Hua Xiao, Chun Yue Feng, Hua Yang Li, Xin Jian Li, Sensors and Actuators B: Chemical 125(2) (2007)651-655; https://doi.org/10.1016/j.snb.2007.03.015
[8] Karimov, K. H., M. M. Ahmed, Z. M. Karieva, M. Saleem, A. Mateen, S. A. Moiz, Sensor Letters. 9(5) (2011)1649-1653; https://doi.org/10.1166/sl.2011.1727
[9] Xia, Yan, Teng Fei, Yuan He, Rui Wang, Fan Jiang,Tong Zhang, Materials Letters 66(1) (2012) 19-21; https://doi.org/10.1016/j.matlet.2011.08.069
[10] Xia, Yan, Yuan He, Rui Wang, Jianchao Feng, Tong Zhang, Materials Letters 88 (2012)43-46; https://doi.org/10.1016/j.matlet.2012.08.038
[11] Tian, Xin, Huitong Cao, Hairong Wang, Jiuhong Wang, Xueyong Wei, Xinyu Wu, Journal of Alloys and Compounds 905 (2022) 164229; https://doi.org/10.1016/j.jallcom.2022.164229
[12] Park, Sunghoon, Hyunsu Kim, Changhyun Jin, Sun-Woo Choi, Sang Sub Kim, Chongmu Lee, Thermochimica acta 542 (2012)69-73; https://doi.org/10.1016/j.tca.2011.12.002
[13] Faudoa-Arzate, Alejandro, Javier Camarillo-Cisneros, Alva Rocío Castillo-González, María Alejandra Favila-Pérez, Renee Joselin Sáenz-Hernández, Paula Rebeca Realyvazquez-Guevara, Carlos Arzate-Quintana, Canadian Journal of Microbiology 67(9) (2021)667-676; https://doi.org/10.1139/cjm-2020-0559
[14] Patil, P. S., S. B. Sadale, S. H. Mujawar, P. S. Shinde, P. S. Chigare, Applied surface science 253(20) (2007) 8560-8567; https://doi.org/10.1016/j.apsusc.2007.04.029
[15] Solis, Jose L., Anders Hoel, Laszlo B. Kish, Claes G. Granqvist, Sami Saukko, Vilho Lantto, Journal of the American Ceramic Society 84(7) (2001)1504-1508; https://doi.org/10.1111/j.1151-2916.2001.tb00868.x
[16] Aguir, K., C. Lemire, D. B. B. Lollman, Sensors and actuators B: Chemical 84(1) (2002)1-5; https://doi.org/10.1016/S0925-4005(02)00003-5
[17] Eranna, G., B. C. Joshi, D. P. Runthala, R. P. Gupta, Critical Reviews in Solid State and Materials Sciences 29(3-4) (2004)111-188; https://doi.org/10.1080/10408430490888977

[18] Gangwar, Amit Kumar, Rahul Godiwal, Stuti Srivastava, Prabir Pal, Govind Gupta, Preetam Singh, Materials Research Bulletin 148 (2022); 111692; https://doi.org/10.1016/j.materresbull.2021.111692

[19] Patil, Dewyani, You-Kyong Seo, Young Kyu Hwang, Jong-San Chang,Pradip Patil, Sensors and Actuators B: Chemical 132(2008)116-124; https://doi.org/10.1016/j.snb.2008.01.021

[20] Pokhrel, Suman, K. S. Nagaraja, Sensors and Actuators B: Chemical 92(1-2) (2003) 144-150; https://doi.org/10.1016/S0925-4005(03)00251-X

[21] Parvatikar, Narsimha, Shilpa Jain, Syed Khasim, M. Revansiddappa, S. V. Bhoraskar, MVN Ambika Prasad, Sensors and Actuators B: Chemical 114(2) (2006) 599-603; https://doi.org/10.1016/j.snb.2005.06.057

[22] Barsan, Nicolae, Udo Weimar, Journal of electroceramics 7(3) (2001)143-167; https://doi.org/10.1023/A:1014405811371

[23] Dai, Ching-Liang, Mao-Chen Liu, Fu-Song Chen, Chyan-Chyi Wu, and Ming-Wei Chang, Sensors and Actuators B: Chemical 123(2) (2007) 896-901; https://doi.org/10.1016/j.snb.2006.10.055

[24] Qu, Wenmin, Wojtek Wlodarski, Sensors and Actuators B: Chemical 64(1-3) (2000) 42-48; https://doi.org/10.1016/S0925-4005(99)00481-5

[25] He, Ziyan, Xu Zhang, Xiaoqin Wei, Dongxiang Luo, Honglong Ning, Qiannan Ye, Renxu Wu, Yao Guo, Rihui Yao, Junbiao Peng, Membranes 12(6) (2022) 590; https://doi.org/10.3390/membranes12060590

[26] Broqvist, Peter,Alfredo Pasquarello, Applied physics letters 89(26) (2006) 262904; https://doi.org/10.1063/1.2424441

[27] Hajnal, Zoltán, József Miró, Gábor Kiss, Ferenc Réti, Péter Deák, Roy C. Herndon, J. Michael Kuperberg, Journal of applied physics 86(7) (1999)3792-3796; https://doi.org/10.1063/1.371289

[28] Chatten, Ryan, Alan V. Chadwick, Aline Rougier, Philip JD Lindan, The Journal of Physical Chemistry B 109(8) (2005)3146-3156; https://doi.org/10.1021/jp045655r

[29] Gillet, M., C. Lemire, E. Gillet, K. Aguir, Surface Science 532 (2003) 519-525; https://doi.org/10.1016/S0039-6028(03)00477-1

[30] Wang, Yong-Lan, Le-Qing Fan, Si-Jia Sun, Jiao-Juan Chen, Zheng-Xue Wu, Ting-Ting Zhu, Yun-Fang Huang, Ji-Huai Wu, Chemical Engineering Journal 428 (2022) 131993; https://doi.org/10.1016/j.cej.2021.131993

[31] Derrar, Khaoula, Mourad Zaabat, Imededdine Zerrouk, Abdelkader Hafdallah, Nouhad Rouabah, Brahim Gasmi, Defect and Diffusion Forum 397 (2019)179-186; https://doi.org/10.4028/www.scientific.net/DDF.397.179

[32] Mondal, Biplob, Borat Basumatari, Jayoti Das, Chirosree Roychaudhury, Hiranmay Saha, Nillohit Mukherjee, Sensors and Actuators B: Chemical 194 (2014) 389-396; https://doi.org/10.1016/j.snb.2013.12.093

[33] Habubi, Nadir F., Ziad M. Abood, Ahmed N. Algamel, International Letters of Chemistry Physics and Astronomy 65 (2016) 81; https://doi.org/10.18052/www.scipress.com/ILCPA.65.80

[34] Mwathe, Patrick, Robinson Musembi, Mathew Munji, Victor Odari, Lawrence Munguti, Alex Ntilakigwa, John Nguu, Boniface Muthoka, Coatings 4(4) (2014) 747-755; https://doi.org/10.3390/coatings4040747

[35] Cho, Yoon Ho, Xishuang Liang, Yun Chan Kang, Jong-Heun Lee, Sensors and actuators B: chemical 207 (2015) 330-337; https://doi.org/10.1016/j.snb.2014.10.001

[36] Rahmane, Saâd, Mohamed Salah Aida, Mohamed Abdou Djouadi, Nicolas Barreau, Superlattices and Microstructures 79 (2015) 148-155; https://doi.org/10.1016/j.spmi.2014.12.001

[37] Abdelkrim, Allag, Saâd Rahmane, Ouahab Abdelouahab, Nadjate Abdelmalek, Gasmi Brahim, Optik 127(5) (2016) 2653-2658; https://doi.org/10.1016/j.ijleo.2015.11.232

[38] Dias, J. S., F. R. M. Batista, R. Bacani, E. R. Triboni, Scientific Reports. 10 (2020)1-11; https://doi.org/10.1038/s41598-020-66043-4

[39] Kuang, Xinliang, Tianmo Liu, Wen Zeng, Xianghe Peng, Zhongchang Wang, Materials Letters 165 (2016) 235-238; https://doi.org/10.1016/j.matlet.2015.10.142

[40] Beaulieu, L. Y., S. D. Beattie, T. D. Hatchard, J. R. Dahn, Journal of the Electrochemical Society 150(4) (2003) A419; https://doi.org/10.1149/1.1556595

[41] Manifacier, J. C., J. Gasiot, J. P. Fillard, Journal of Physics E: Scientific Instruments 9(11) (1976)1002; https://doi.org/10.1088/0022-3735/9/11/032

[42] Mcguire, K., Z. W. Pan, Z. L. Wang, D. Milkie, Jose Menendez, A. M. Rao, Journal of nanoscience and nanotechnology 2(5) (2002) 499-502; https://doi.org/10.1166/jnn.2002.129

[43] Lee Jae-Hyeong, Thin solid films 515(15) (2007) 6089-6093; https://doi.org/10.1016/j.tsf.2006.12.097

[44] Jang, Dong Mi, Hyuck Jung, Nguyen Duc Hoa, Dojin Kim, Soon-Ku Hong, Hyojin Kim, Journal of Nanoscience and Nanotechnology 12(2) (2012) 1425-1428; https://doi.org/10.1166/jnn.2012.4656

[45] Mehraj, Sumaira, M. Shahnawaze Ansari, Physica E: Low-Dimensional Systems and Nanostructures 65 (2015) 84-92; https://doi.org/10.1016/j.physe.2014.08.016

[46] Thangadurai, P., A. Chandra Bose, S. Ramasamy, R. Kesavamoorthy, T. R. Ravindran, Journal of Physics and Chemistry of Solids 66(10) (2005) 1621-1627; https://doi.org/10.1016/j.jpcs.2005.05.079

[47] Khan, Abdul Faheem, Mazhar Mehmood, A. M. Rana, M. T. Bhatti, A. Mahmood, Chinese Physics Letters 26(7) (2009) 077803; https://doi.org/10.1088/0256-307X/26/7/077803

[48] Lee, N., R. D. Hartschuh, D. Mehtani, A. Kisliuk, J. F. Maguire, M. Green, M. D. Foster, A. P. Sokolov, Journal of Raman Spectroscopy 8(6) (2007) 789-796; https://doi.org/10.1002/jrs.1698

[49] Saito, Yuika, Masashi Motohashi, Norihiko Hayazawa, Satoshi Kawata, Journal of microscopy 229(2) (2008) 217-222; https://doi.org/10.1111/j.1365-2818.2008.01889.x

[50] Traylor, Joseph Gibson, H. G. Smith, R. M. Nicklow, M. K. Wilkinson, Physical Review B 3(10) (1971) 3457; https://doi.org/10.1103/PhysRevB.3.3457

[51] Tazikeh, Simin, Amir Akbari, Amin Talebi, Emad Talebi, Materials Science-Poland 32(1) (2014) 98-101; https://doi.org/10.2478/s13536-013-0164-y

[52] Elango, Ganesh, Selvaraj Mohana Roopan, Journal of Photochemistry and Photobiology B: Biology 155 (2016) 34-38; https://doi.org/10.1016/j.jphotobiol.2015.12.010

[53] Juliasih, N., I. Noviandri, In IOP Conference Series: Materials Science and Engineering 188(1) (2017) 012025; https://doi.org/10.1088/1757-899X/188/1/012025

[54] Roguai, S., A. Djelloul, Algerian Journal of Environmental Science and Technology. 8 (2022).

[55] Bastami, H., E. Taheri-Nassaj, Journal of alloys and compounds 495 (2010) 121-125; https://doi.org/10.1016/j.jallcom.2010.01.099

[56] Jouhannaud, J., J. Rossignol, D. Stuerga, Journal of Solid State Chemistry 181(6) (2008) 1439-1444; https://doi.org/10.1016/j.jssc.2008.02.040

[57] Nachiar, R. Ariya, S. Muthukumaran, Optics & Laser Technology 112 (2019) 458-466; https://doi.org/10.1016/j.optlastec.2018.11.055

[58] Jahnavi, V. Siva, Sumanta Kumar Tripathy, Physica B: Condensed Matter 565 (2019) 61-72; https://doi.org/10.1016/j.physb.2019.04.020

[59] Velásquez, C., F. Rojas, M. L. Ojeda, A. Ortiz, A. Campero, Nanotechnology 16(8) (2005) 1278; https://doi.org/10.1088/0957-4484/16/8/049

[60] Amalric-Popescu, D., F. Bozon-Verduraz, Catalysis today 70(1-3) (2001) 139-154; https://doi.org/10.1016/S0920-5861(01)00414-X

[61] Entradas, T., J. F. Cabrita, S. Dalui, M. R. Nunes, O. C. Monteiro, António Jorge Silvestre, Materials Chemistry and Physics 147(3) (2014) 563-571; https://doi.org/10.1016/j.matchemphys.2014.05.032

[62] Tripathy, Sumanta Kumar, Bhabani Prasad Hota, P. V. Rajeswari, Bulletin of Materials Science 36(7) (2013) 1231-1237; https://doi.org/10.1007/s12034-013-0582-9

[63] Palanichamy, S., L. Amalraj J. Raj Mohamed, PS Satheesh Kumar, South Asian Journal of Engineering and Technology 2 (2016) 26-34.

[64] Tripathy, Sumanta Kumar, Bhabani Prasad Hota, P. V. Rajeswari, Bulletin of Materials Science 36(7) (2013) 1231-1237; https://doi.org/10.1007/s12034-013-0582-9

[65] Tripathy, Sumanta Kumar, Bhabani Prasad Hota, P. V. Rajeswari, Bulletin of Materials Science 36(7) (2013) 1231-1237.

[66] Roguai, Sabrina, Abdelkader Djelloul, Applied Physics A 125(12) (2019) 1-11; https://doi.org/10.1007/s00339-019-3118-3

[67] Melsheimer, J., D. Ziegler, Thin Solid Films129(1-2) (1985) 35-47; https://doi.org/10.1016/0040-6090(85)90092-6

[68] Ajili, Mejda, Michel Castagné, Najoua Kamoun Turki, Optik 126(7-8) (2015) 708-714; https://doi.org/10.1016/j.ijleo.2015.02.039

[69] Beensh-Marchwicka, G., L. Kròl-Stępniewska, A. Misiuk, Thin Solid Films 113(3) (1984) 215-224; https://doi.org/10.1016/0040-6090(84)90224-4

[70] De Waal, H_, F. Simons, Thin Solid Films 77(1-3) (1981) 253-258; https://doi.org/10.1016/0040-6090(81)90380-1

[71] Shamala, K. S., L. C. S. Murthy, K. Narasimha Rao, Materials Science and Engineering: B 106(3) (2004) 269-274; https://doi.org/10.1016/j.mseb.2003.09.036

[72] Khanna, V. K., R. K. Nahar, Sensors and Actuators 5(3) (1984) 187-198; https://doi.org/10.1016/0250-6874(84)80009-8

[73] Nahar, R. K., V. K. Khanna, International Journal of Electronics Theoretical and Experimental 52(6) (1982) 557-567; https://doi.org/10.1080/00207218208901467

[74] Qian, Jingwen, Zhijian Peng, Zhenguang Shen, Zengying Zhao, Guoliang Zhang, Xiuli Fu, Scientific reports 6 (2016) 1-9; https://doi.org/10.1038/srep25574

[75] Hajnal, Zoltán, József Miró, Gábor Kiss, Ferenc Réti, Péter Deák, Roy C. Herndon, J. Michael Kuperberg, Journal of applied physics 86(7) (1999) 3792-3796; https://doi.org/10.1063/1.371289

[76] Yuk, J., & Troczynski, T, Sensors and Actuators B: Chemical 94(3) (2003) 290-293; https://doi.org/10.1016/S0925-4005(03)00371-X

[77] Li, Wei, Juyan Liu, Chao Ding, Gang Bai, Jie Xu, Qingying Ren, Jinze Li, Sensors 17(10) (2017) 2392; https://doi.org/10.3390/s17102392

[78] Liu, Ming-Qing, Cong Wang, Nam-Young Kim, Sensors 17(2) (2017) 284; https://doi.org/10.3390/s17020284

[79] Ansari, Reza, E-Journal of Chemistry 3(4) (2006)186-201; https://doi.org/10.1155/2006/860413

[80] Matsuguchi, M., Kuroiwa, T., Miyagishi, T., Suzuki, S., Ogura, T., & Sakai, Y, Sensors and actuators B: Chemical 52(1-2) (1998) 53-57; https://doi.org/10.1016/S0925-4005(98)00255-X